Letters in Applied NanoBioScience
Open-Access Journal (ISSN: 2284-6808)

Article
Volume 15, Issue 3, 2026, 92
https://doi.org/10.33263/LIANBS153.092

Dihydropyrimidinones as Potential Direct Renin Inhibitors: *In Silico* Molecular Docking and Molecular Dynamics Approach

Era Erg Bamba [1], Mark Tristan Quimque [2,3,*]

[1] Department of Chemistry, College of Mathematics and Natural Sciences, Caraga State University, Butuan City, Caraga 8600, Philippines
[2] Department of Chemistry, College of Science and Mathematics, Mindanao State University-Iligan Institute of Technology, Iligan City, Region X 9200, Philippines
[3] Drug Design and Development Related Research Laboratory, Premier Research Institute of Science and Mathematics, Mindanao State University-Iligan Institute of Technology, Iligan City, Region X 9200, Philippines
* Correspondence: marktristan.quimque@g.msuiit.edu.ph;

Received: 13.10.2024; Accepted: 28.02.2026; Published: 02.07.2026

Abstract: This study contributes to ongoing efforts to address the global health challenge of hypertension by in silico exploring new inhibitors of the renin-angiotensin-aldosterone system (RAAS). Renin, a key enzyme regulator in this pathway, was selected as the molecular target for treatment intervention. Specifically, the potential of dihydropyrimidinone (DHPM) derivatives as direct renin inhibitors was investigated using the enzyme's crystal structure (PDB ID: 2V0Z. A total of 440 compounds with substitutions at N1, N3, and C4 of the DHPM core were evaluated through molecular docking. Top-scoring ligands for each substitution type were further assessed through molecular dynamics simulations. Pharmacokinetic properties, including absorption, distribution, metabolism, and excretion (ADME), were predicted using SwissADME, while toxicity risks were assessed with OSIRIS Property Explorer. Compounds 30j and 33h emerged as promising candidates, showing strong binding affinities and favorable pharmacokinetic profiles. Molecular dynamics confirmed the stability of these compounds within the renin complex throughout the simulation period. These results support the potential of DHPM derivatives as lead compounds for the development of new renin-targeted antihypertensive therapies.

Keywords: hypertension; pyrimidinones; direct renin inhibitor; molecular docking; molecular dynamics simulation.

1. Introduction

Hypertension is among the leading health problems, contributing significantly to morbidity and mortality worldwide through its association with stroke, heart failure, renal failure, atherosclerosis, and, more recently, dementia [1-6]. Despite advancements in medical treatments, hypertension remains inadequately managed, with approximately half of the individuals who have hypertension being unaware of their condition, and roughly half of those diagnosed are not receiving sufficient treatment [7-9]. The renin-angiotensin-aldosterone system (RAAS) plays a major role in the pathophysiology and development of hypertension [10], especially in patients with comorbidities such as diabetes, kidney diseases, or heart

failure. Within this cascade, renin catalyzes the rate-limiting step, the conversion of angiotensinogen to angiotensin I - making [11]. Recent preclinical studies emphasize the effectiveness of disrupting the renin-angiotensin-aldosterone system at multiple points, demonstrating this strategy as an effective strategy for lowering blood pressure. Inhibition of renin, the enzyme responsible for the cleavage of angiotensinogen to angiotensin I, which is the first and rate-limiting step of the RAAS pathway, should then afford the maximum blood pressure-lowering effect [12, 13]. Furthermore, it is believed that renin inhibition is an appealing approach for effectively blocking the RAAS and should have fewer mechanism-related side effects than current therapies targeting downstream events in the RAAS pathway [14]. Currently, aliskiren remains the sole direct renin inhibitor commercially available [15], highlighting the need for novel compounds with improved efficacy and pharmacological profiles. 3,4-Dihydropyrimidin-2(1H)-ones (DHPMs) and their derivatives are heterocyclic compounds known for their broad spectrum of biological activities, including antihypertensive effects [16]. Given their structural versatility and pharmacological potential, this study investigates a series of DHPM derivatives through in silico analyses to evaluate their potential as direct renin inhibitors. Additionally, pharmacokinetic properties and toxicity profiles were assessed to support rational lead optimization and guide future drug development.

2. Materials and Methods

2.1. Target protein selection and preparation.

The structure of human renin (PDB ID:2V0Z) was obtained from the RCSB Protein Data Bank at a high resolution in three dimensions. The protein was added to the UCSF Chimera platform for further analysis. To prepare the protein for docking studies, missing hydrogen atoms were added, and appropriate charges were assigned using the Gasteiger charge method through Amber's Antechamber module computation. The structure was minimized to optimize its conformation for docking experiments [17].

2.2. Ligand selection and preparation.

A collection of 440 dihydropyrimidinone compounds with good synthetic accessibility was employed, of which 400 underwent alkylation at positions N1 and N3. These ligands were designed to potentially have a strong interaction with the enzyme renin. The molecular structures of the ligands were generated using ChemDraw Professional 16.0. For ligand presentation in docking studies, Avogadro (Version 1.2.0), an open-source molecular builder, was used to optimize ligand structures and convert them to PDB files [18]. The optimization process involved using the UFF force field and the steepest descent algorithm.

2.3. Molecular docking studies.

Molecular docking analyses were performed using Autodock Vina as the primary docking algorithm. The three-dimensional structures of human renin and its ligands were added to the docking platform in PDB format. While performing the molecular docking simulations, the "flexible ligand into the flexible site" experimental protocol was implemented. In this protocol, each ligand could be flexibly positioned within a pre-computed grid box within the ligand-binding cavity of the proteins, using COACH algorithms [19, 20]. Following the BFGS (Broyden-Fletcher-Goldfarb-Shanno) algorithm of AutoDock Vina

(Version 1 1.2), all docking parameters were maintained at default values as the molecular docking simulation was performed [21]. After each simulation, Autodock Vina displays a set of docking poses with determined binding affinities for each ligand. To represent the set, the docking pose with the highest affinity was recorded and subjected to post-dock analysis.

2.4. Molecular dynamics simulations (MDS).

To further evaluate the dynamic behavior of the ligands with the highest docking scores, molecular dynamics (MD) simulations were performed using GROMACS version 2020.1 on an Ubuntu Linux platform. The topology of the renin crystal structure was generated using the CHARMM36 force field in combination with the TIP3P water model. For the ligands, topology parameters were obtained using the CHARMM General Force Field (CGenFF). The protein-ligand complex was subsequently solvated in a docahedral simulation box filled with single-point charge (SPC) water molecules. System neutrality was achieved by adding Na^+ and Cl^- counterions. Energy minimization was then carried out to stabilize the system using descent algorithm for 5,000 steps. Long-range electrostatic and van der Waals interactions were treated using the particle mesh Ewald (PME) method. [22]. After equilibration, a total of 50 ns simulation was done for each system, maintaining the temperature at 300 K. During the production phase, trajectory frames were saved at 10 ps intervals. These trajectories were subsequently analyzed to determine the root mean square deviation (RMSD), root mean square fluctuation (RMSF), and radius of gyration (Rg) for each simulated system. The interaction energies between the renin enzyme and the ligands were determined using the g_energy analysis tool of GROMACS version 2020.1 from the 50 ns trajectory data. The interaction energy (IE) of the top binding complexes was taken as the sum of the Coulomb and Lennard-Jones short-range energies ($E_{Coul\text{-}SR}$ and $E_{LJ\text{-}SR}$) [23, 24].

2.5. Druggability, pharmacokinetic, toxicity, and ADME prediction.

The SwissADME computational software was used to predict absorption, distribution, metabolism, and excretion (ADME) properties [25]. The "rule of five" by Lipinski was used to evaluate the biochemical characteristics of each ligand in the SwissADME data set and to determine the pharmacokinetic characteristics that may influence its absorption and permeation across cell membranes. Physicochemical properties of each ligand that may affect its absorption and permeability across cellular membranes were evaluated. Drug-likeness was assessed using Lipinski's rule of five, which suggests that compounds are more likely to exhibit good oral bioavailability when at least three of the following criteria are satisfied: <500 Daltons (Da) for molecular weight, <5 for calculated lipophilicity (MLogP), <10 for the number of hydrogen bond acceptors, and <5 for the number of hydrogen bond donors. Furthermore, the OSIRIS Property Explorer software was utilized to predict the toxicity of the hit compounds. This prediction considered factors such as mutagenicity, tumorigenicity, reproductive toxicity, and irritating effects. The same program was used to forecast solubility (LogS), where LogS ≥ -4 denotes good solubility and favorable chemical absorption [26].

3. Results and Discussion

3.1. Ligand selection and molecular docking analysis.

A total of 440 dihydropyrimidinone compounds with varying substitutions around the pyrimidinone core, particularly C4 arylation (Figure S1) and N1/N3 alkylation (Figures S2-S12), were subjected to virtual molecular docking screening against renin (PDBID: 2V0Z). For the C4-arylated compounds, the molecular docking results showed that the DHPM derivatives displayed high affinity for the renin enzyme, with binding affinities ranging from -6.5 to -9.9 kcal/mol (Table 1). Notably, compound 26, with a binding energy of -8.5 kcal/mol, showed comparable, if not better, affinity to that of the reference drug, aliskiren.

Given the interesting results and the interest in designing new DHPMs, further substitutions at the N1 (coded a-i) and N3 (coded j-k) positions of compounds 1-40 were explored to enhance binding interactions. Among the N1-alkylated derivatives, compound 33h incorporates a 4-(α-hexylcinnamyl) substituent and a 2-hydroxyethyl group at N1, exhibiting the highest binding affinity, recording a value of -9.9 kcal/mol. The presence of longer, more complex alkyl groups suggests enhanced hydrophobic interactions and increased conformational stability, which contribute to improved binding efficiency. Additionally, the presence of a 2-hydroxyethyl group at the N1 position provides additional hydrogen-bonding potential, facilitating polar interactions with surrounding residues and further stabilizing the ligand-protein complex. Meanwhile, compound 30j, which features a 4-(β-phenylcinnamyl) substituent and a methyl propanoate attachment at the N3 position, displays the best binding onto renin for the N3-alkylated derivatives with a binding affinity of -8.2 kcal/mol. The synergistic effects of the hydrophobic phenyl group and polar ester functionality indicate that both hydrophobic and polar interactions are crucial for optimized binding. Overall, the results indicate a clear pattern: the introduction of larger, hydrophobic substituents at both N1 and N3 positions significantly enhances binding affinity. This improvement is likely due to increased interactions with the target site, as well as the potential for functional groups to engage in hydrogen bonding and other polar interactions. Systematic exploration of various substituent combinations based on their steric and electronic properties may further advance the design of potent DHPM derivatives.

The 3D and 2D protein-ligand interactions critical to the affinity were analyzed (Table 2, Figure 1). Renin, an aspartic protease, utilizes a catalytic dyad consisting of two similar domains, each containing an aspartic acid residue, Asp38 and Asp226 in human renin. The active site of the renin molecule is located within the cleft between its two homologous lobes, a configuration critical to its catalytic function [27]. This dyad structure enables the enzyme to efficiently convert angiotensinogen into angiotensin I, underscoring its role in blood pressure regulation. For aliskiren, binding affinity analysis highlights the conventional hydrogen-bonding interaction between the catalytic dyad (Asp38 and Asp226) and the hydroxy moiety. Compound 33h conferred the highest binding affinity of -9.9 kcal/mol, with the following interactions observed in 2V0Z's active site: carbon-hydrogen bonding interaction with Thr18 and Gly228, π-sulfur interaction with Met303, alkyl/π-alkyl interactions with Pro118, Ala229, Phe124, and Val36. Binding affinity analysis highlights a carbon-hydrogen interaction with Gly40, which is also observed in aliskiren. Compound 30j demonstrated a binding affinity of –8.2 kcal/mol. It formed a conventional hydrogen bond with Ser230, carbon-hydrogen bonding with Gly40, a π-sulfur interaction with Met303, a π–

π T-shaped interaction with Tyr231, and multiple hydrophobic contacts involving Val36, Phe124, and Ala229. The repeated interaction with Gly40 highlights its possible role as a key anchoring residue in renin-ligand recognition. Overall, these interaction profiles indicate that the top-binding DHPM derivatives effectively engage critical residues within the renin active site, particularly Gly40, Met303, and Val36. The overlap of these interactions with those observed in the reference inhibitor aliskiren suggests that the DHPM scaffold has the potential to mimic established binding modes, reinforcing its promise as a lead structure for further development of direct renin inhibitors.

Table 1. Binding affinities of DHPM derivatives 1-40 against renin.

Compound Code	Binding Energy	Compound Code	Binding Energy
1	-7.0	**21**	-7.0
2	-6.9	**22**	-7.2
3	-8.5	**23**	-7.0
4	-7.3	**24**	-7.0
5	-7.4	**25**	-6.9
6	-7.2	**26**	-8.5
7	-6.6	**27**	-7.3
8	-7.1	**28**	-7.4
9	-7.2	**29**	-7.2
10	-7.2	**30**	-6.6
11	-7.2	**31**	-7.1
12	-7.3	**32**	-7.2
13	-6.8	**33**	-7.5
14	-7.2	**34**	-7.5
15	-6.8	**35**	-7.6
16	-7.1	**36**	-7.5
17	-6.5	**37**	-7.8
18	-6.6	**38**	-8.1
19	-7.1	**39**	-7.2
20	-6.8	**40**	-7.2

Table 2. Summary of docking interactions for the renin enzyme by the top two ligands.

Ligand	Ligand/receptor docking interaction	Binding affinity (kcal/mol)	Interpretations
30j	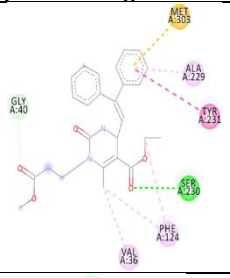	-8.2	Conventional hydrogen bonding interaction with Ser230, carbon hydrogen bonding interaction with Gly40, π-sulfur interaction with Met303, π-π T-shaped interaction with Tyr231, alkyl/π-alkyl interaction with Val36, Phe124 and Ala229
33h	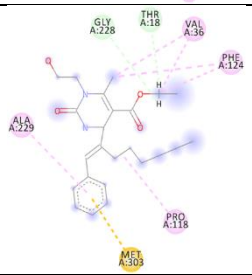	-9.9	Carbon-hydrogen bonding interaction with Thr18 and Gly228, π-sulfur interaction with Met303, alkyl/π-alkyl interactions with Pro118, Ala229, Phe124 and Val36
aliskiren	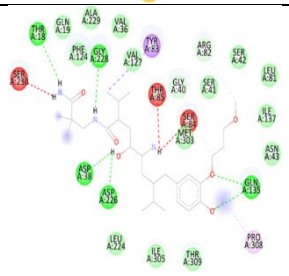	-8.4	Conventional hydrogen bonding interactions with Asp38, Asp226, Thr18, Gly228, and Gln135, carbon hydrogen bonding interactions with Gly40 and Arg82, unfavorable donor-donor interactions with Ser84, Ser230, and Thr85, π-σ interaction with Tyr83, alkyl interaction with Pro308

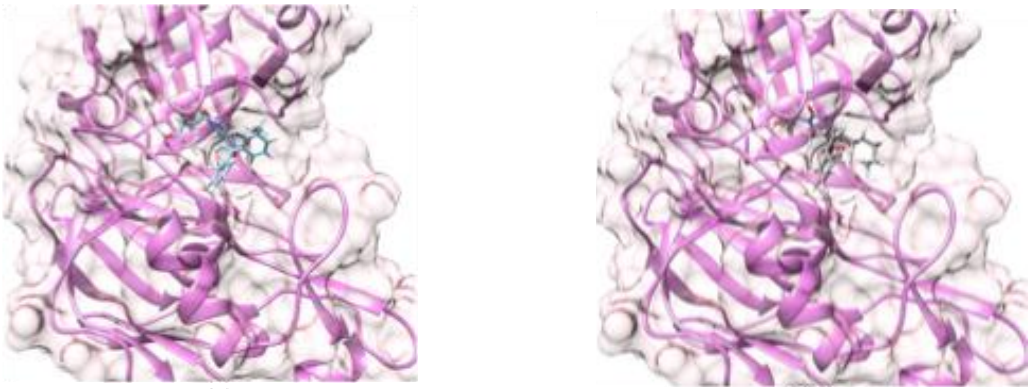

(a) **(b)**

Figure 1. (a) Docked pose of compound 30j against renin receptor shown as ribbon representation; **(b)** docked pose of compound 33h against renin receptor shown as ribbon representation.

3.2. ADME analysis, toxicity, and medicinal chemistry friendliness.

SWISSADME was employed to evaluate the drug-likeness and pharmacokinetic properties of the top-binding DHPM derivatives, compounds 30j and 33h, providing a preliminary assessment of their suitability as drug candidates. Based on Lipinski's Rule of Five, which serves as a standard guideline for oral drug-likeness, both compounds exhibited no violations. This rule evaluates key physicochemical properties—lipophilicity (Log P), molecular weight (MW), hydrogen bond donors (HBD), and hydrogen bond acceptors (HBA)—to predict oral bioavailability. The parameters listed in Table 3 adhere to the structural limitations that ligands must conform to interact effectively with the protein target. The absence of violations suggests that both 30j and 33h are likely to be orally bioavailable and possess acceptable pharmacokinetic behavior for further development [28].

Table 3. Lipinski's rule of five for absorption, distribution, metabolism, and excretion (ADME) analysis and druglikeness.

Compound	Lipinski's rule of 5			Druglikeness
	Properties	Value	Violations	
30j	Molecular weight (< 500Da)	448.51 g/mol	0	YES
	MLogP (< 5)	3.04		
	H-bond donor (< 5)	1		
	H-bond acceptor (< 10)	5		
	Rotatable bonds (< 5)	10		
33h	Molecular weight (< 500Da)	414.54 g/mol	0	YES
	MLogP (< 5)	2.91		
	H-bond donor (< 5)	2		
	H-bond acceptor (< 10)	4		
	Rotatable bonds (< 5)	12		

The BOILED-Egg model was used to predict passive gastrointestinal absorption (HIA) and blood–brain barrier (BBB) permeability. This graphical method plots lipophilicity (WLOGP) against topological polar surface area (TPSA) to categorize compounds based on their predicted permeation characteristics. According to the plot (Figure 2), compound 33h was located in the yellow yolk region, indicating a strong probability of BBB penetration, but outside the white region, signifying poor GI absorption. Moreover, it was not a substrate of P-glycoprotein (P-gp), suggesting a lower risk of active efflux and potentially higher CNS exposure. In contrast, compound 30j appeared in the white region, indicating good GI absorption, but outside the yolk, implying limited BBB permeation. Like 33h, it is also not a P-gp substrate, supporting favorable systemic exposure [29].

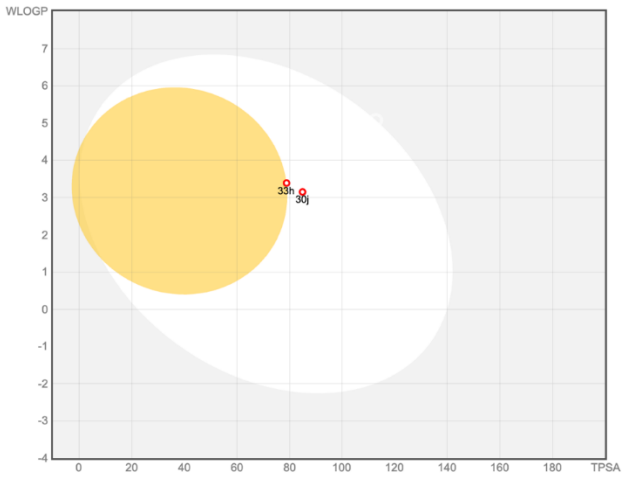

Figure 2. Prediction of gastrointestinal (GI) tract and brain permeation by the brain or intestinal estimated permeation predictive model (BOILED-Egg) method.

Moreover, the compounds were subjected to toxicity prediction using the OSIRIS Property Explorer, a tool that estimates the potential safety risks based on known substructures associated with toxicity (Table 4). The analysis focused on four key endpoints: mutagenicity, tumorigenicity, irritation, and reproductive effects. This assessment revealed that compound **30j** carries a high risk of toxicity for reproductive effects due to its ethyl dibenzyl moiety, while showing no indications of mutagenic, tumorigenic, or irritant toxicity. In addition, compound **33h** demonstrated a notable level of toxicity towards tumor formation or growth, with moderate irritant toxicity. Compound **33h** was predicted to be tumorigenic and irritant due to its urea core with 2-hydroxyethyl and 3-methyl attachment moieties. Furthermore, both compounds displayed optimal water solubility, as evidenced by their LogS values of -4.49 and -4.38, respectively. When all other physicochemical parameters were considered, both ligands met general drug-likeness criteria, though further structural refinement is recommended to improve their safety profiles.

Table 4. Toxicity risks of compounds **33h** and **30j** as predicted by OSIRIS property explorer.

Compound	Toxicity risk				Solubility (LogS)
	Mutagenic	Tumorigenic	Irritant	Reproductive effective	
30j	None	None	None	High risk	-4.49
33h	None	High risk	Medium risk	None	-4.38

3.3. Molecular dynamic simulations.

To evaluate the stability and dynamic behavior of the renin-ligand complexes, a comprehensive analysis of multiple molecular dynamics (MD) parameters was performed, including root mean square deviation (RMSD), root mean square fluctuation (RMSF), radius of gyration (Rg), and interaction energies (IE) over a 50 ns simulation period. The RMSD analysis (Figure 3) revealed distinct dynamic behavior between the two top-scoring ligands, compounds **30j** and **33h**. The renin-33h complex exhibited consistently lower RMSD values, ranging from 1.8 to 2.2 Å throughout the simulation. This narrow fluctuation indicates early stabilization and sustained conformational equilibrium, suggesting that compound 33h rapidly adopts and maintains a stable binding pose within the active site. In contrast, the renin-30j complex initially showed comparable RMSD values but began to increase gradually beyond 30 ns, reaching approximately 3.5 Å. This upward trend suggests that while 30j eventually stabilizes in the early phase, the complex undergoes larger conformational shifts or slight rearrangements at later stages. Nevertheless, the RMSD profile remained within acceptable

limits for biological macromolecules, suggesting that the renin structure retained its overall integrity.

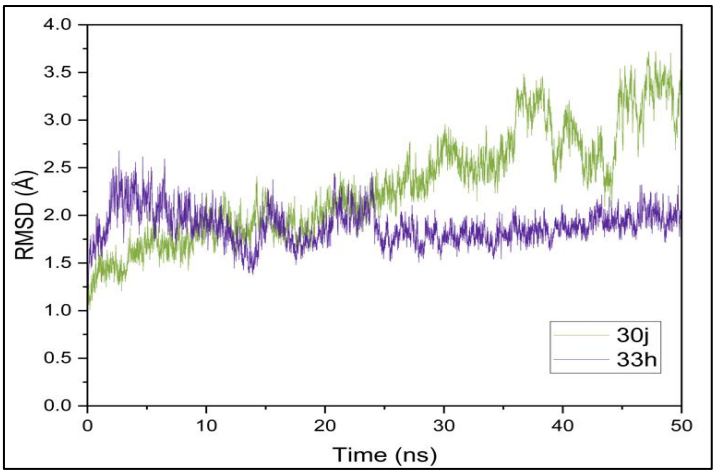

Figure 3. RMSD (Å) as a function of time (ns) of the top-binding ligands.

To complement the RMSD results, the radius of gyration (Rg) [30] was examined to assess global compactness of the protein-ligand complexes (Figure 4). Both complexes maintained Rg values around 20 Å, with minimal deviations, indicating the preservation of a tightly folded structure throughout the simulation.

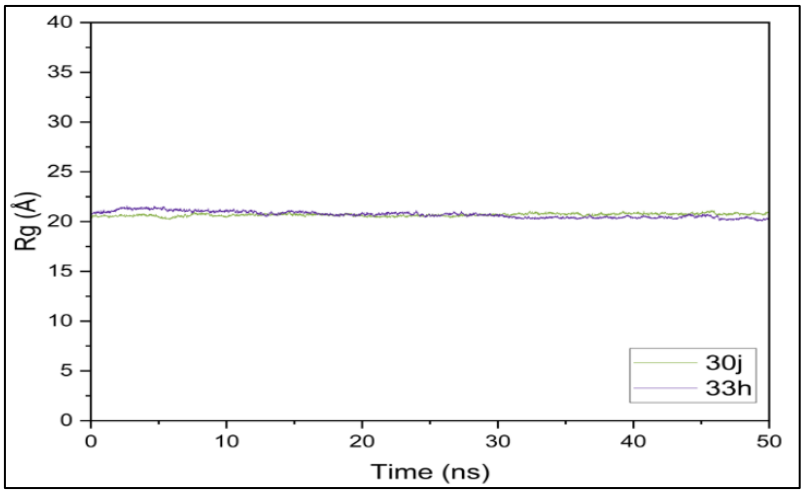

Figure 4. The Rg (Å) as a function of time of the top binding ligands.

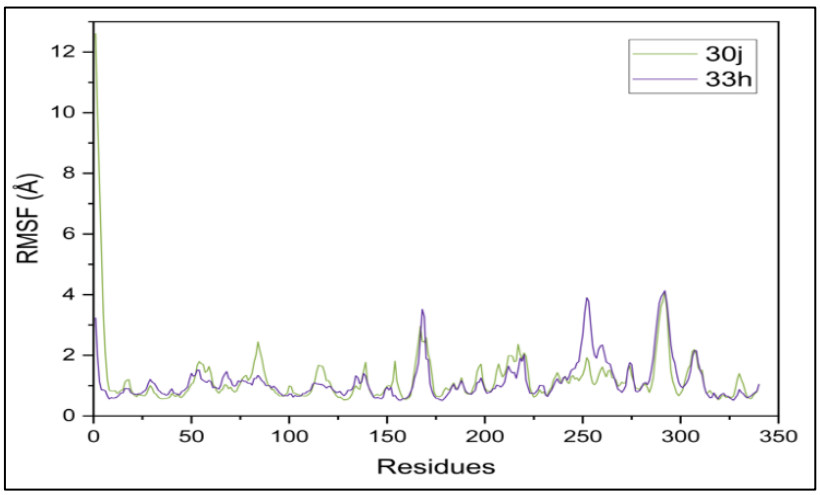

Figure 5. Time-averaged, residual RMSF (Å) of the top binding ligands.

Notably, compound 30j exhibited slightly smoother Rg behavior than 33h during the first half of the run, although 33h quickly converged to a similarly stable profile. This consistent Rg trend, despite the increasing RMSD of 30j in later frames, suggests that the conformational fluctuations were likely localized rather than indicative of global unfolding. These findings are supported by the RMSF analysis (Figure 5), which showed low per-residue fluctuations across the protein backbone. The observed flexibility was largely confined to the loop region between residues 250–300, a feature typical of solvent-exposed or dynamic segments. Both complexes showed similar RMSF profiles, supporting the interpretation that ligand binding did not disrupt renin's overall secondary or tertiary structure.

Further reinforcing these structural insights, the protein-ligand interaction energy **(IE)** analysis indicated that compound **33h** exhibited the most favorable binding energetics, with a total IE of –204.52 kcal/mol, comprising significant Coulombic (–74.58 ± 4.4 kcal/mol) and Lennard-Jones (–129.94 ± 4.4 kcal/mol) contributions. The strong electrostatic and van der Waals interactions support the early and sustained RMSD stability observed in the renin-33h complex. In comparison, compound **30j** had a slightly lower IE of –190.29 kcal/mol, with dominant van der Waals interactions (–146.16 ± 0.86 kcal/mol) and weaker Coulombic forces (–44.13 ± 6.4 kcal/mol). The relative instability in the RMSD profile of 30j may reflect minor rearrangements required to optimize these predominantly hydrophobic contacts within the binding pocket.

Table 5. Average protein-ligand interaction energy (IE) from a 50-ns trajectory of the top-binding complexes.

Compound	Energy terms, kcal/mol		
	Coulomb-SR	Lennard Jones-SR	IE
30j	-44.1275 ± 6.4	-146.161 ± 0.86	-190.2885
33h	-74.5829 ± 4.4	-129.938 ± 4.4	-204.5208

4. Conclusions

The results identify dihydropyrimidinone (DHPM) derivatives as promising candidates for direct renin inhibition, targeting the renin-angiotensin-aldosterone system (RAAS) catalytic dyad. Through a combination of molecular docking and molecular dynamics simulations, specific compounds, such as 30j and 33h, demonstrated strong and stable interactions with renin, supported by favorable pharmacokinetic profiles. Overall, this virtual screening of DHPM derivatives against renin provided evidence to continue in vitro investigations of these compounds to further assess their potential as direct renin inhibitors, as part of ongoing efforts to discover new antihypertensive agents.

Supplementary materials

The supplementary materials associated with this article are available here: **Download**

Author Contributions

Conceptualization, EEB and MTQ; formal analysis, EEB and MTQ; investigation, EEB and MTQ; writing—original draft preparation, EEB; writing—review and editing, MTQ; visualization, EEB; supervision, MTQ. All authors have read and agreed to the published version of the manuscript.

Institutional Review Board Statement

Not applicable.

Informed Consent Statement

Not applicable.

Data Availability Statement

Data supporting the findings of this study are available upon reasonable request from the corresponding author.

Funding

This research was funded by the Department of Science and Technology-Accelerated Science and Technology Human Resource and Development Program (DOST-ASTHRDP).

Acknowledgments

Special thanks are extended to the Drug Design and Development Related Research and the Premier Research Institute of Science and Mathematics at Mindanao State University-Iligan Institute of Technology. The authors also extend their sincere appreciation to Mark Ruben de Belen for his invaluable assistance in the docking procedures and simulations. The contributions of each author and co-author to this manuscript are wholeheartedly acknowledged.

Conflicts of Interest

The authors declared no potential conflict of interest.

References

1. Burnier, M.; Damianaki, A. Hypertension as Cardiovascular Risk Factor in Chronic Kidney Disease. *Circ. Res.* **2023**, *132*, 1050-1063, https://doi.org/10.1161/circresaha.122.321762.
2. Hengel, F.E.; Benitah, J.-P.; Wenzel, U.O. Mosaic theory revised: inflammation and salt play central roles in arterial hypertension. *Cell. Mol. Immunol.* **2022**, *19*, 561-576, https://doi.org/10.1038/s41423-022-00851-8.
3. Cheon, E.-J. Hypertension and cognitive dysfunction: a narrative review. *J. Yeungnam Med. Sci.* **2023**, *40*, 225-232, https://doi.org/10.12701/jyms.2022.00605.
4. Kario, K.; Mogi, M.; Hoshide, S. Latest hypertension research to inform clinical practice in Asia. *Hypertens. Res.* **2022**, *45*, 555-572, https://doi.org/10.1038/s41440-022-00874-8.
5. Law, J.P.; Pickup, L.; Pavlovic, D.; Townend, J.N.; Ferro, C.J. Hypertension and cardiomyopathy associated with chronic kidney disease: epidemiology, pathogenesis and treatment considerations. *J. Hum. Hypertens.* **2023**, *37*, 1-19, https://doi.org/10.1038/s41371-022-00751-4.
6. Mulligan, M.D.; Murphy, R.; Reddin, C.; Judge, C.; Ferguson, J.; Alvarez-Iglesias, A.; McGrath, E.R.; O'Donnell, M.J. Population attributable fraction of hypertension for dementia: global, regional, and national estimates for 186 countries. *eClinicalMedicine* **2023**, *60*, 102012, https://doi.org/10.1016/j.eclinm.2023.102012.
7. Boateng, E.B.; Ampofo, A.G. A glimpse into the future: modelling global prevalence of hypertension. *BMC Public Health* **2023**, *23*, 1906, https://doi.org/10.1186/s12889-023-16662-z.
8. Elattar, K.M.; Mert, B.D.; Monier, M.; El-Mekabaty, A. Advances in the chemical and biological diversity of heterocyclic systems incorporating pyrimido[1,6-*a*]pyrimidine and pyrimido[1,6-*c*]pyrimidine scaffolds. *RSC Adv.* **2020**, *10*, 15461-15492, https://doi.org/10.1039/d0ra00411a.

9. Tinawi, M. New Trends in the Diagnosis and Management of Hypertension. *Cureus* **2022**, *14*, e22393, https://doi.org/10.7759/cureus.22393.
10. Nwia, S.M.; Leite, A.P.O.; Li, X.C.; Zhuo, J.L. Sex differences in the renin-angiotensin-aldosterone system and its roles in hypertension, cardiovascular, and kidney diseases. *Front. Cardiovasc. Med.* **2023**, *10*, 1198090, https://doi.org/10.3389/fcvm.2023.1198090.
11. Ortiz, R.M.; Satou, R.; Zhuo, J.L.; Nishiyama, A. The Renin-Angiotensin-Aldosterone System in Metabolic Diseases and Other Pathologies. *Int. J. Mol. Sci.* **2023**, *24*, 7413, https://doi.org/10.3390/ijms24087413.
12. Gunawardhana, K.L.; Hong, L.; Rugira, T.; Uebbing, S.; Kucharczak, J.; Mehta, S.; Karunamuni, D.R.; Cabera-Mendoza, B.; Gandotra, N.; Scharfe, C.; Polimanti, R.; Noonan, J.P.; Mani, A. A systems biology approach identifies the role of dysregulated PRDM6 in the development of hypertension. *J. Clin. Invest.* **2023**, *133*, e160036, https://doi.org/10.1172/jci160036.
13. Ueno, M.; Fujii, W.; Ono, W.; Murata, H.; Fujigaki, Y.; Shibata, S. Renin Inhibition and the Long-Term Renal Function in Patients With Hypertensive Emergency: A Retrospective Cohort Study. *Am. J. Hypertens.* **2024**, *37*, 407-414, https://doi.org/10.1093/ajh/hpad099.
14. Nakamura, Y.; Fujimoto, T.; Ogawa, Y.; Sugita, C.; Miyazaki, S.; Tamaki, K.; Takahashi, M.; Matsui, Y.; Nagayama, T.; Manabe, K.; Mizuno, M.; Masubuchi, N.; Chiba, K.; Nishi, T. Discovery of DS-8108b, a Novel Orally Bioavailable Renin Inhibitor. *CS Med. Chem. Lett.* **2012**, *3*, 754-758, https://doi.org/10.1021/ml300168e.
15. Wood, J.M.; Maibaum, J.; Rahuel, J.; Grütter, M.G.; Cohen, N.-C.; Rasetti, V.; Rüger, H.; Göschke, R.; Stutz, S.; Fuhrer, W.; Schilling, W.; Rigollier, P.; Yamaguchi, Y.; Cumin, F.; Baum, H.-P.; Schnell, C.R.; Herold, P.; Mah, R.; Jensen, C.; O'Brien, E.; Stanton, A.; Bedigian, M.P. Structure-based design of aliskiren, a novel orally effective renin inhibitor. *Biochem. Biophys. Res. Commun.* **2003**, *308*, 698-705, https://doi.org/10.1016/s0006-291x(03)01451-7.
16. Sánchez-Sancho, F.; Escolano, M.; Gaviña, D.; Csáky, A.G.; Sánchez-Roselló, M.; Díaz-Oltra, S.; del Pozo, C. Synthesis of 3,4-Dihydropyrimidin(thio)one Containing Scaffold: Biginelli-like Reactions. *Pharmaceuticals* **2022**, *15*, 948, https://doi.org/10.3390/ph15080948.
17. Wang, Y.; Khan, A.; Chandra Kaushik, A.; Junaid, M.; Zhang, X.; Wei, D.-Q. The systematic modeling studies and free energy calculations of the phenazine compounds as anti-tuberculosis agents. *J. Biomol. Struct. Dyn.* **2019**, *37*, 4051-4069, https://doi.org/10.1080/07391102.2018.1537896.
18. de Leon, V.N.O.; Manzano, J.A.H.; Pilapil, D.Y.H.; Fernandez, R.A.T.; Ching, J.K.A.R.; Quimque, M.T.J.; Agbay, J.C.M.; Notarte, K.I.R.; Macabeo, A.P.G. Anti-HIV reverse transcriptase plant polyphenolic natural products with in silico inhibitory properties on seven non-structural proteins vital in SARS-CoV-2 pathogenesis. *J. Genet. Eng. Biotechnol.* **2021**, *19*, 104, https://doi.org/10.1186/s43141-021-00206-2.
19. Yang, J.; Roy, A.; Zhang, Y. Protein–ligand binding site recognition using complementary binding-specific substructure comparison and sequence profile alignment. *Bioinformatics* **2013**, *29*, 2588-2595, https://doi.org/10.1093/bioinformatics/btt447.
20. Quimque, M.T.J.; Notarte, K.I.R.; Fernandez, R.A.T.; Mendoza, M.A.O.; Liman, R.A.D.; Lim, J.A.K.; Pilapil, L.A.E.; Ong, J.K.H.; Pastrana, A.M.; Khan, A.; Wei, D.-Q.; Macabeo, A.P.G. Virtual screening-driven drug discovery of SARS-CoV2 enzyme inhibitors targeting viral attachment, replication, post-translational modification and host immunity evasion infection mechanisms. *J. Biomol. Struct. Dyn.* **2021**, *39*, 4316-4333, https://doi.org/10.1080/07391102.2020.1776639.
21. Trott, O.; Olson, A.J. AutoDock Vina: Improving the speed and accuracy of docking with a new scoring function, efficient optimization, and multithreading. *J. Comput. Chem.* **2010**, *31*, 455-461, https://doi.org/10.1002/jcc.21334.
22. Toukmaji, A.; Sagui, C.; Board, J.; Darden, T. Efficient particle-mesh Ewald based approach to fixed and induced dipolar interactions. *J. Chem. Phys.* **2000**, *113*, 10913-10927, https://doi.org/10.1063/1.1324708.
23. Van Der Spoel, D.; Lindahl, E.; Hess, B.; Groenhof, G.; Mark, A.E.; Berendsen, H.J.C. GROMACS: Fast, flexible, and free. *J. Comput. Chem.* **2005**, *26*, 1701-1718, https://doi.org/10.1002/jcc.20291.
24. Santos, J.; Quimque, M.T.; Liman, R.A.; Agbay, J.C.; Macabeo, A.P.G.; Corpuz, M.J.-A.; Wang, Y.-M.; Lu, T.-T.; Lin, C.-H.; Villaflores, O.B. Computational and Experimental Assessments of Magnolol as a Neuroprotective Agent and Utilization of UiO-66(Zr) as Its Drug Delivery System. *ACS Omega* **2021**, *6*, 24382-24396, https://doi.org/10.1021/acsomega.1c02555.

25. Kaliaperumal, K.; Salendra, L.; Liu, Y.; Ju, Z.; Sahu, S.K.; Elumalai, S.; Subramanian, K.; M. Alotaibi, N.; Alshammari, N.; Saeed, M.; Karunakaran, R. Isolation of anticancer bioactive secondary metabolites from the sponge-derived endophytic fungi *Penicillium* sp. and *in-silico* computational docking approach. *Front. Microbiol.* **2023**, *14*, 1216928, https://doi.org/10.3389/fmicb.2023.1216928.
26. Phukhamsakda, C.; Macabeo, A.P.G.; Huch, V.; Cheng, T.; Hyde, K.D.; Stadler, M. Sparticolins A–G, Biologically Active Oxidized Spirodioxynaphthalene Derivatives from the Ascomycete *Sparticola junci*. *J. Nat. Prod.* **2019**, *82*, 2878-2885, https://doi.org/10.1021/acs.jnatprod.9b00604.
27. Danser, A.H.J.; Deinum, J. Renin, Prorenin and the Putative (Pro)renin Receptor. *Hypertension* **2005**, *46*, 1069-1076, https://doi.org/10.1161/01.hyp.0000186329.92187.2e.
28. Lipinski, C.A.; Lombardo, F.; Dominy, B.W.; Feeney, P.J. Experimental and computational approaches to estimate solubility and permeability in drug discovery and development settings. *Adv. Drug Deliv. Rev.* **2001**, *46*, 3-26, https://doi.org/10.1016/s0169-409x(00)00129-0.
29. Daina, A.; Michielin, O.; Zoete, V. SwissADME: a free web tool to evaluate pharmacokinetics, drug-likeness and medicinal chemistry friendliness of small molecules. *Sci. Rep.* **2017**, *7*, 42717, https://doi.org/10.1038/srep42717.
30. Mosquera-Yuqui, F.; Lopez-Guerra, N.; Moncayo-Palacio, E.A. Targeting the 3CLpro and RdRp of SARS-CoV-2 with phytochemicals from medicinal plants of the Andean Region: molecular docking and molecular dynamics simulations. *J. Biomol. Struct. Dyn.* **2022**, *40*, 2010-2023, https://doi.org/10.1080/07391102.2020.1835716.

Publisher's Note & Disclaimer